

# ON ESTIMATING THE HIGH-ENERGY CUTOFF IN THE X-RAY SPECTRA OF BLACK HOLES VIA REFLECTION SPECTROSCOPY

JAVIER A. GARCÍA<sup>1</sup>, THOMAS DAUSER<sup>2</sup>, JAMES F. STEINER<sup>1</sup>, JEFFREY E. MCCLINTOCK<sup>1</sup>, MASON L. KECK<sup>1,3</sup>, JÖRN WILMS<sup>2</sup>

*Draft version October 29, 2021*

## ABSTRACT

The fundamental parameters describing the coronal spectrum of an accreting black hole are the slope  $\Gamma$  of the power-law continuum and the energy  $E_{\text{cut}}$  at which it rolls over. Remarkably, this latter parameter can be accurately measured for values as high as 1 MeV by modeling the spectrum of X-rays reflected from a black hole accretion disk at energies below 100 keV. This is possible because the details in the reflection spectrum, rich in fluorescent lines and other atomic features, are very sensitive to the spectral shape of the hardest coronal radiation illuminating the disk. We show that by fitting simultaneous *NuSTAR* (3–79 keV) and low-energy (e.g., *Suzaku*) data with the most recent version of our reflection model **relxill** one can obtain reasonable constraints on  $E_{\text{cut}}$  at energies from tens of keV up to 1 MeV, for a source as faint as 1 mCrab in a 100 ks observation.

**Keywords:** accretion, accretion disks – atomic processes – black hole physics

## 1. INTRODUCTION

X-ray reflection spectroscopy is currently our most effective tool for probing accretion processes and space-time near the supermassive black holes that power active galactic nuclei (AGN). In the current paradigm, the power-law continuum is produced either in a central hot corona (e.g., Shakura & Sunyaev 1973; Haardt 1993) or at the base of a jet (e.g., Matt et al. 1992; Markoff et al. 2005). A fraction of this radiation illuminates the accretion disk and is reprocessed into a rich reflection spectrum consisting of fluorescent lines and other features, which provides detailed information on the composition and ionization state of the accretion disk and constraints on the structure of the corona. Importantly, reflection spectroscopy of AGN is *the* way to infer the spin of their black holes via modeling key spectral features, such as the Fe K line ( $\sim 6.4$ – $6.9$  keV), the Fe K edge ( $\sim 7$ – $8$  keV), and the Compton hump ( $\sim 20$ – $40$  keV). Observational data suggest that in many cases the illuminating power-law continuum cuts off abruptly in the hard X-ray band (e.g., Zdziarski et al. 2000). Most X-ray detectors are unable to accurately constrain this cutoff energy because they either have limited sensitivity at high-energies or none at all. Thus, reflection models have been traditionally simplified by adopting a fixed cutoff energy at a reasonable value, e.g.,  $E_{\text{cut}} = 300$  keV (Ross & Fabian 2005; García & Kallman 2010).

The 2012 launch of *NuSTAR* (Harrison et al. 2013) has revolutionized reflection spectroscopy because its instruments provide both very low background and superb sensitivity over the band 3–79 keV, which captures all the key reflection features (e.g., Risaliti et al. 2013; Walton

et al. 2013; Parker et al. 2014). The quality of the *NuSTAR* data demand reflection models that properly treat the high-energy cutoff as a fit parameter. We have developed advanced relativistic models of X-ray reflection from ionized accretion disks; the most recent version is **relxill** (García et al. 2014). These models include a rich atomic database, full treatment of the angular distribution of the reflected radiation, and an improved geometrical model of the illuminating coronal source. Furthermore, the most recent version of **relxill** also includes the high-energy cutoff  $E_{\text{cut}}$  as a fit parameter. Likewise,  $E_{\text{cut}}$  is included as a free parameter in the most recent version of the reflection code **relionx** (Ross & Fabian 2005).

In the standard picture, the power law spectrum is generated in the corona by Compton up-scattering of thermal disk photons. The shape of the spectrum depends on the geometry, temperature, and optical depth of the corona (e.g., Rybicki & Lightman 1979). In particular, the fractional energy change of a scattered photon (in the non-relativistic limit)

$$\frac{\Delta E}{E} = \frac{4kT_e}{m_e c^2} - \frac{E}{m_e c^2} \quad (1)$$

implies a cutoff of the power-law near  $4kT_e$  because the energy gained by the photon cannot exceed the energy of the electron (e.g., Titarchuk 1994). In practice,  $E_{\text{cut}} \sim 2 - 3kT_e$  due to dispersion, geometrical, and relativistic effects (e.g., Petrucci et al. 2001). Thus, an empirical estimate of  $E_{\text{cut}}$  provides direct information on the temperature  $T_e$  of the coronal electrons.

The recent data obtained with *NuSTAR* has spotlighted  $E_{\text{cut}}$  (e.g., Brenneman et al. 2014; Ballantyne et al. 2014; Marinucci et al. 2014; Baloković et al. 2015). In most of these studies, the coverage of *NuSTAR* to 79 keV was sufficient to directly observe the roll over of the power-law component ( $E_{\text{cut}} \sim 50 - 200$  keV). However, fitting a *NuSTAR* spectrum of NGC 5506 with relativistic reflection models, Matt et al. (2015) surprisingly found  $E_{\text{cut}} = 720^{+130}_{-190}$  keV. Likewise, in fitting a

<sup>1</sup> Harvard-Smithsonian Center for Astrophysics, 60 Garden St., Cambridge, MA 02138 USA; javier@head.cfa.harvard.edu, jem@cfa.harvard.edu, jsteiner@head.cfa.harvard.edu

<sup>2</sup> Dr. Karl Remeis-Observatory and Erlangen Centre for Astroparticle Physics, Sternwartstr. 7, 96049 Bamberg, Germany; thomas.dauser@sternwarte.uni-erlangen.de

<sup>3</sup> Institute for Astrophysical Research, Boston University, 725 Commonwealth Avenue, Boston, MA 02215, USA; keckm@bu.edu

*Suzaku*+*NuSTAR* spectrum of NGC 4151 Keck et al. (2015) found that a value of  $E_{\text{cut}}$  near 1 MeV was statistically required.

In this Letter, we demonstrate the remarkable ability of reflection models to provide strong constraints on  $E_{\text{cut}}$  up to several hundred keV, values that greatly exceed the limit of the detector bandpass (e.g., 79 keV for *NuSTAR*). While not detected directly, this high-energy portion of the spectrum conditions the ionization state and structure of the disk atmosphere, which in turn modifies the observed reflection features. Thus, by properly modeling the reflection component at moderate energies, one can accurately estimate  $E_{\text{cut}}$  at extreme energies and thereby constrain the physical properties of the corona.

## 2. MODELING THE REFLECTION SPECTRUM

The reflection model **relxill** is a fusion of our reflection code **xillver** (García & Kallman 2010; García et al. 2013) and **relline** (Dauser et al. 2010, 2013), which is a general-relativistic ray tracing code. We first describe the atomic physics part **xillver**, which assumes plane-parallel geometry and idealizes the disk as a slab with a total optical depth of  $\tau = 10$  and a constant density of  $n = 10^{15} \text{ cm}^{-3}$ . The illuminating source is assumed to have a power-law spectrum with a photon index  $\Gamma$  and an exponential cutoff at high energies,  $E_{\text{cut}}^4$ . The intensity of the illumination is controlled by specifying the ionization parameter:

$$\xi = \frac{4\pi F_x}{n}, \quad (2)$$

where  $F_x$  is the net ionizing flux in the energy band 1–1000 Ry. A comprehensive grid of models has been calculated and provided to the community for fitting observational data that cover a wide range of model parameters. The most recent version of **xillver** includes models for several different values of the high-energy cutoff, namely,  $E_{\text{cut}} = 20, 50, 80, 100, 150, 200, 250, 300, 500, 1000 \text{ keV}$ . In Figure 1 we show examples of models for these values of  $E_{\text{cut}}$  for two ionization parameters,  $\log \xi = 1$  and  $\log \xi = 3$ .

As illustrated in Figure 1 and discussed in García et al. (2013),  $E_{\text{cut}}$  controls the intensity and shape of the illuminating spectrum and thereby affects the global reflection spectrum. The Compton hump is most dramatically affected, its peak shifting to lower energies as  $E_{\text{cut}}$  decreases. Weaker effects are seen at lower energies ( $\lesssim 10 \text{ keV}$ ), which are mostly driven by changes in the ionization state of the gas. As Equation 2 suggests, two models with the same ionization parameter (and hence the same  $F_x$ ) but different values of  $E_{\text{cut}}$  will give rise to distinctive reflection spectra. This difference occurs because the illuminating spectrum with lower  $E_{\text{cut}}$  will have a significantly larger proportion of its photons concentrated at lower energies, which favors photoelectric interactions over electron scattering relative to the spectrum with high  $E_{\text{cut}}$ .

Changes in  $E_{\text{cut}}$  and the consequent shift in the balance of photons in the hard and soft bands affects the ionization structure of the slab, as illustrated in the two right

panels of Figure 1. On the one hand, for low ionization the lower values of  $E_{\text{cut}}$  (strong soft flux) produce hotter atmospheres; as a consequence, in this regime the temperature is mainly regulated by photoionization heating and recombination cooling. On the other hand, for high ionization the hotter atmospheres correspond to higher values of  $E_{\text{cut}}$  (strong hard flux); in this regime, the temperature is controlled by electron scattering of the abundant hard photons. Finally, we stress that despite the opposing trends in the temperature profiles shown in Figure 1, for a fixed value of  $\xi$  the reflected spectrum is always softer for smaller  $E_{\text{cut}}$ .

To produce the complete relativistic model **relxill**, we convolve spectra computed along the disk using **xillver** with the general-relativistic ray tracing code **relline** (Dauser et al. 2010, 2013). The model **relxill** self-consistently calculates the angle-dependent, relativistic ionized reflection spectra (García et al. 2014) that are used in fitting data. Figure 2 shows reflected spectra (and the incident power-law spectra) for  $\log \xi = 1$  calculated with **relxill**. For clarity, we show only two models, for  $E_{\text{cut}}=300 \text{ keV}$  and  $E_{\text{cut}}=1 \text{ MeV}$ . These are the same as the corresponding two models shown in the top-left panel of Figure 1, except that here the spectral features are blurred by Doppler and gravitational-redshift effects.

The lower panel in Figure 2 shows the ratio of the  $E_{\text{cut}}=300 \text{ keV}$  model to the  $E_{\text{cut}}=1 \text{ MeV}$  model and also the ratio of the incident power-law spectra. In the *NuSTAR* band, while the two models can be distinguished by considering either the power-law or the reflected component, it is the stronger curvature of the reflected component that is more telling. At lower energies, in the *Suzaku* band, the power-law is incapable of distinguishing between the two models because the continuum is essentially identical (apart from the normalization). On the other hand, the reflected component shows significant changes in spectral features, which sharply distinguish the models. Thus, whether one considers *NuSTAR* alone, or *NuSTAR* plus *Suzaku*, it is possible to constrain  $E_{\text{cut}}$  at energies far above the bandpass of the detector, but in either case it is the reflected component that carries the greater weight.

## 3. FITS TO SIMULATED *NuSTAR* DATA

We first demonstrate that *NuSTAR* data alone can provide strong constraints on  $E_{\text{cut}}$ . To this end, we simulate data using appropriate response and background files<sup>5</sup>, assuming a circular extraction region with  $60''$  radius centered  $1'$  off axis. We combine the data from both *NuSTAR* telescopes (focal plane modules FPMA and FPMB) and simulate spectra for an exposure time of 100 ks.

We consider sources, both extragalactic and Galactic, with intensities/fluxes that cover the range normally encountered in practice. Using the ISIS package (Houck & Denicola 2000), we grouped the data so that the minimum signal-to-noise ratio for each bin was 5 to ensure the soundness of our  $\chi^2$  analysis. We additionally grouped the data to ensure appropriate sampling, given that the resolution of the *NuSTAR* detectors is 0.4/0.9 keV at 6/60 keV. Specifically, we further binned the simulated

<sup>4</sup> For simplicity, we use a phenomenological e-folded power-law model rather than a proper model of thermal Comptonization such as that of Zdziarski et al. (2003), a model whose accuracy has been demonstrated (e.g., Gierlinski et al. 1997; Wardziński et al. 2002).

<sup>5</sup> [http://www.nustar.caltech.edu/page/response\\_files](http://www.nustar.caltech.edu/page/response_files)

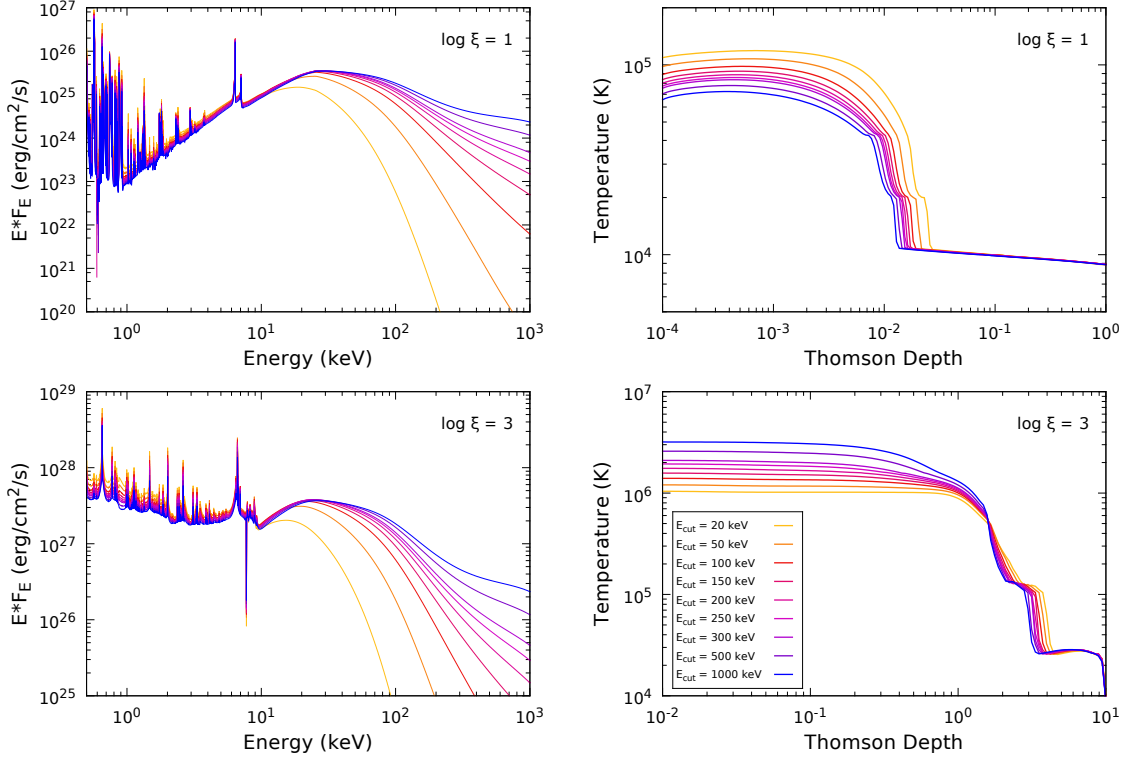


**Figure 1.** The left panels show *xillver* reflection spectra for  $\log \xi = 1$  (top) and  $\log \xi = 3$  (bottom) and for nine values of  $E_{\text{cut}}$  (see legend in lower-right panel). For all models, the illuminating spectrum is a power law with index  $\Gamma = 2$  and the iron abundance is solar. For simplicity we only show angle-averaged spectra (García et al. 2014). The right panels show the temperature profile in the slab.

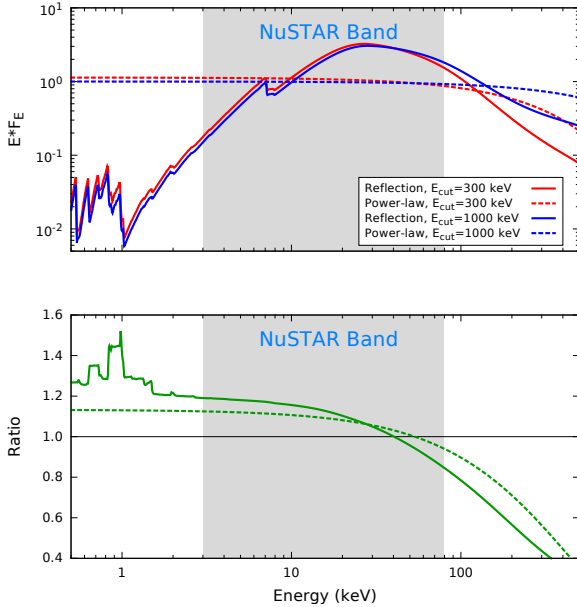


**Figure 2.** *Top:* Relativistically blurred reflection spectra (solid lines) computed using *relxill* for  $\log \xi = 1$  and the respective power-law spectra (dashed lines) of the illuminating source with slope  $\Gamma = 2$ . The red curves are for  $E_{\text{cut}} = 300$  keV and the blue curves for  $E_{\text{cut}} = 1$  MeV. *Bottom:* Ratio of the  $E_{\text{cut}} = 300$  keV spectra to the  $E_{\text{cut}} = 1$  MeV spectra. The ratio of the reflection/power-law spectra is plotted as a solid/dashed line. The shaded box spans the *NuSTAR* bandpass (3–79 keV).

data, which have uniform bin widths of 0.04 keV over the entire energy band, to 0.2 keV and 0.4 keV for energies

below and above 20 keV, respectively<sup>6</sup>.

In the simulations, we used the model *Tbabs\*relxill* (Section 2), where *Tbabs* models the interstellar absorption (Wilms et al. 2000). We simulated spectra for eleven values of the high-energy cutoff ranging from 50 keV to 1 MeV. The other model parameters, which are the same for all simulations, are: the hydrogen column density  $N_{\text{H}} = 5 \times 10^{21} \text{ cm}^{-2}$ ; dimensionless spin parameter  $a = cJ/GM^2 = 0.998$ ; emissivity index  $q = 3$ ; inclination of the disk  $i = 45$  deg; inner disk radius  $R_{\text{in}} = R_{\text{ISCO}}$ ; power-law  $\Gamma = 2$ ; ionization parameter  $\log \xi = 1$ ; iron abundance  $A_{\text{Fe}} = 1$ ; and the reflection fraction  $R_f = 3$ , which is defined as the ratio of the reflected to the power-law flux in the 20–40 keV band. Our calculations in this instance do not link the reflection fraction to the emissivity index, which would require specifying the geometry of the reflector and the illuminating source.

We emphasize that this Letter deals exclusively with relativistically-blurred reflection by ionized gas in the very inner portion of the accretion disk for which the reflection fraction can vary widely, with values ranging from a few tenths to  $> 20$  for rapidly spinning black holes (Dauser et al. 2014). Reflection in this regime is not to be confused with reflection by distant, neutral material, which is observed in the spectra of many sources and is usually modeled using the *pexrav* model (e.g., Zdziarski et al. 1999, 2003).

We generated the simulated spectra using the *fakeit* task in *XSPEC* v-12.8.2b (Arnaud 1996), and we then fit

<sup>6</sup> We found that binning the data to a few samples per resolution element is important: Without this binning, the fitted values of  $E_{\text{cut}}$  were consistently biased below the input. This result suggests more generally that fitting oversampled data is not good practice.

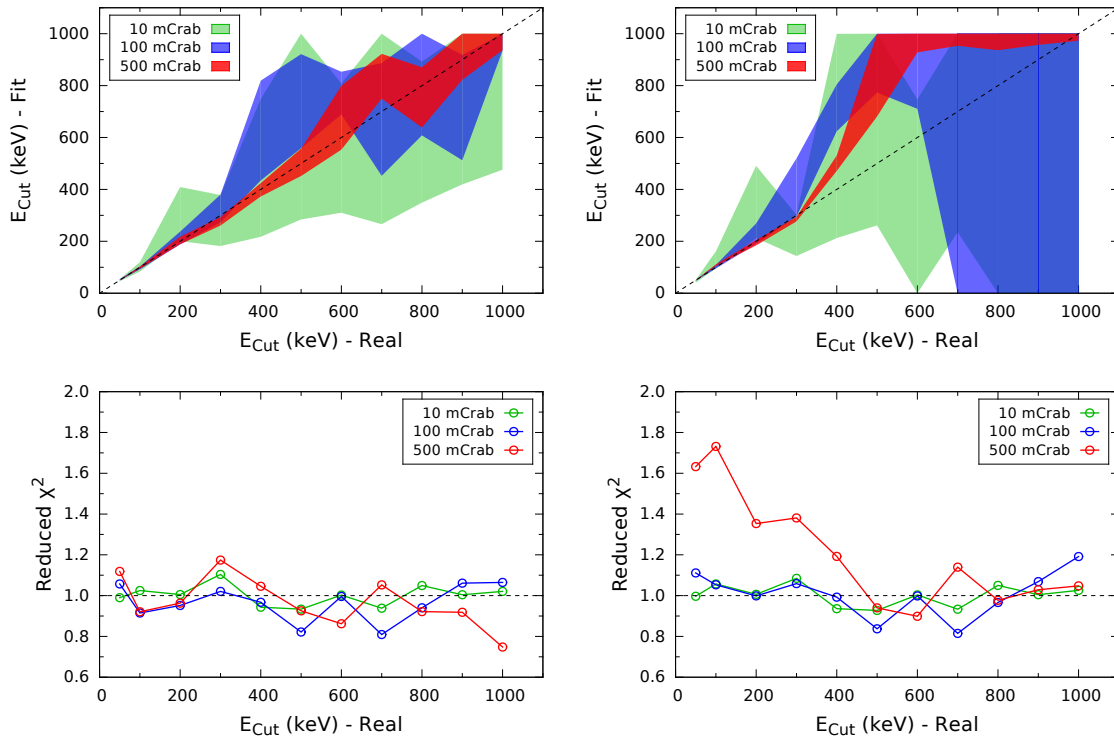


**Figure 3.** Results of fitting simulated *NuSTAR* data. *Top:* Shown plotted are the values of  $E_{\text{cut}}$  returned by the fits compared to the values of  $E_{\text{cut}}$  used in producing the simulated data for three assumed values of source intensity (see legend). Fits using Model 1 (left panel) demonstrate that  $E_{\text{cut}}$  can be accurately recovered for energies far above the 79 keV limit of the *NuSTAR* bandpass. Meantime, the very poor performance of Model 2 (right panel) is obvious. Error bars are at the 90% level of confidence. *Bottom:* Goodness of fit; note the poor performance of Model 2 at low to moderate values of  $E_{\text{cut}}$  for the brightest source.

ted these spectra using two different models, with  $E_{\text{cut}}$ ,  $\Gamma$ ,  $\xi$ ,  $A_{\text{Fe}}$ , normalization, and  $R_f$  free to vary:

**Model 1: *Tbabs\*relxill*.** We first employ the same model used to produce the simulated data in order to evaluate how well the parameters,  $E_{\text{cut}}$  in particular, can be recovered.

**Model 2: *Tbabs\*highcut\*relxill*.** In this case, the parameter  $E_{\text{cut}}$  in *relxill* is fixed at 1 MeV, while it is allowed to vary freely in *highcut*, a simple exponential convolution model acting on *relxill*. Model 2 aims to test how accurately  $E_{\text{cut}}$  is recovered when the spectrum is described by modifying the high-energy region of an otherwise incorrect reflection model (i.e., when ignoring the effects on the disk’s ionization structure described in § 2).

Results of fitting the simulated data are shown in Figure 3. The top panels show the fitted values of  $E_{\text{cut}}$  versus the values used in simulating the data, with results for Model 1/2 in the left/right panel. The shaded regions indicate uncertainties at the 90% confidence level. The colors are keyed to source intensity. The quality of the fits is indicated in the lower panels.

Focusing on the results for Model 1 (top-left panel) and the 10 mCrab source, which delivers  $1.8 \times 10^6$  counts in the *NuSTAR* band, the recovered values of  $E_{\text{cut}}$  below 400 keV are of marginal quality, while above that energy they only provide lower limits on  $E_{\text{cut}}$ . However, for source intensities of  $\sim 100 - 500$  mCrab ( $\sim 10^7 - 10^8$  counts), significantly better performance is achieved. We conclude that for high-quality data one can determine the high-energy cutoff with reasonable preci-

sion using *NuSTAR* data alone.

Turning to the results for Model 2 (top-right panel), one immediately sees the much poorer performance achieved in attempting to recover  $E_{\text{cut}}$  by simply fitting the curvature in the power-law continuum component using the *highcut* model. As mentioned in Section 1, this was the standard approach used before  $E_{\text{cut}}$  was included as a fit parameter in reflection models. The *highcut* model provides constraints of reasonable quality only for  $E_{\text{cut}} < 300$  keV. Furthermore, for the brightest source considered (500 mCrab), Model 2 yields unsatisfactory results for  $E_{\text{cut}} > 300$  keV because not only is  $E_{\text{cut}}$  significantly over-predicted, the error bars are also misleadingly small. Interestingly, at lower energies the quality of the fits are worse for the brightest source (Figure 3, bottom-right panel). Other model parameters are also poorly constrained, e.g., the Fe abundance is grossly underestimated, while both the power-law index and the reflection fraction  $R_f$  are over-predicted.

Importantly, we note that Models 1 and 2 give the same quality of fit (with the exception of the 500 mCrab simulation for low  $E_{\text{cut}}$ ) so that a  $\chi^2$ -test does not generally promote one model over the other. However, as we have demonstrated, Model 2 returns incorrect estimates of the parameters in all cases. In short, *good statistical precision does not ensure that the parameter values returned by a fit to a model are reliable or physically meaningful.*

#### 4. INCLUDING LOW-ENERGY DATA

Figure 2 indicates that the low-energy component ( $E \lesssim 3$  keV) of the reflection spectrum is more sensitive to the value of  $E_{\text{cut}}$  than the component in the *NuSTAR*

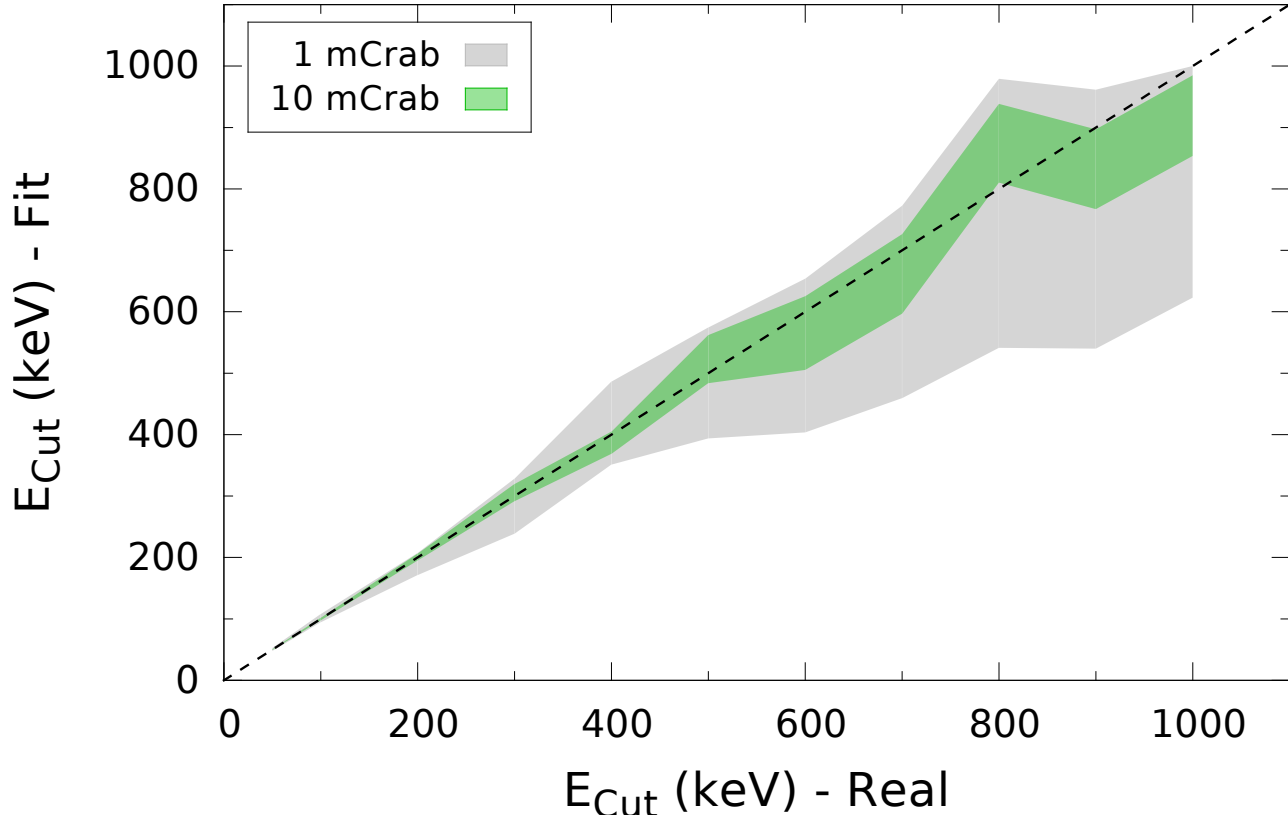


**Figure 4.** Including low-energy *Suzaku* data, Model 1 delivers extraordinary performance in constraining  $E_{\text{cut}}$  out to extreme energies compared to using *NuSTAR* data alone. The results shown here of fitting simulated data for a 10 mCrab source are superior to those obtained for a 500 mCrab source using only *NuSTAR* data (see the upper-left panel in Figure 3).

band. Therefore, we now consider spectra comprised of *Suzaku* plus *NuSTAR* data in the expectation that this will significantly improve the constraints on  $E_{\text{cut}}$ , and the other parameters as well. The simulated low-energy data are prepared using *Suzaku* response files, the same set of model parameters, and the same source fluxes as those used in preparing the *NuSTAR* data.

In the following, we consider only Model 1. Fitting the combined set of *Suzaku* (0.5–8 keV) and *NuSTAR* (3–79 keV) simulated spectra, we obtain the outstanding result shown in Figure 4. The fit for the 10 mCrab source is incomparably better than for the *NuSTAR* data alone (compare upper-left panel of Figure 3). The high-energy cutoff is strongly constrained for all values of  $E_{\text{cut}}$  considered; even at 1 MeV, the error is only about 7%. This excellent performance of our reflection model is a consequence of the sensitivity of the reflection component to changes in the high-energy portion of the illuminating spectrum (Figure 2). These simulations clearly demonstrate that fits to features in the relatively low-energy portion of the spectrum, where the instruments are most sensitive, can deliver accurate measurements of  $E_{\text{cut}}$  at energies far beyond the limit of the detector bandpass.

Also shown in Figure 4 are the results for a 1 mCrab source ( $2 \times 10^5$  counts). Remarkably, with the inclusion of low-energy data even  $\sim 10^5$  counts are sufficient to recover  $E_{\text{cut}}$  with reasonable precision; the error bars for  $E_{\text{cut}} > 600$  keV are  $\sim 30\%$ .

Finally, with two additional simulations we demonstrate that the reflection component is much more important in constraining  $E_{\text{cut}}$  than the power law. For the same 1 mCrab source, and including *Suzaku* data, Figure 5 compares the performance of a cutoff power-law model alone (`cutoffpl`) with a pure reflection model. These two limiting cases can be compared directly to the intermediate case of our adopted composite model (i.e., power law plus reflection) with  $R_f = 3$  shown in gray in Figure 4. The three cases considered together show that stronger reflection translates into a better constraint on  $E_{\text{cut}}$ .

## 5. DISCUSSION AND CONCLUSIONS

We have demonstrated that our reflection model `relxill` can constrain the physically important coronal parameter  $E_{\text{cut}}$  for spectra with intensities like those encountered in observations of AGN. We have furthermore shown that attempting to constrain  $E_{\text{cut}}$  by imposing a cutoff that is external to the reflection model yields relatively poor constraints on  $E_{\text{cut}}$ . Such a simplified model inaccurately represents the observed spectrum and introduces strong biases in the values inferred for the key physical parameters.

We analyzed two simulated data sets using `relxill`: (1) With *NuSTAR* data alone (3–79 keV),  $E_{\text{cut}} \gtrsim 400$  keV can only be constrained if the spectrum contains  $\gtrsim 10^7$  counts, which is infeasible for most observations of

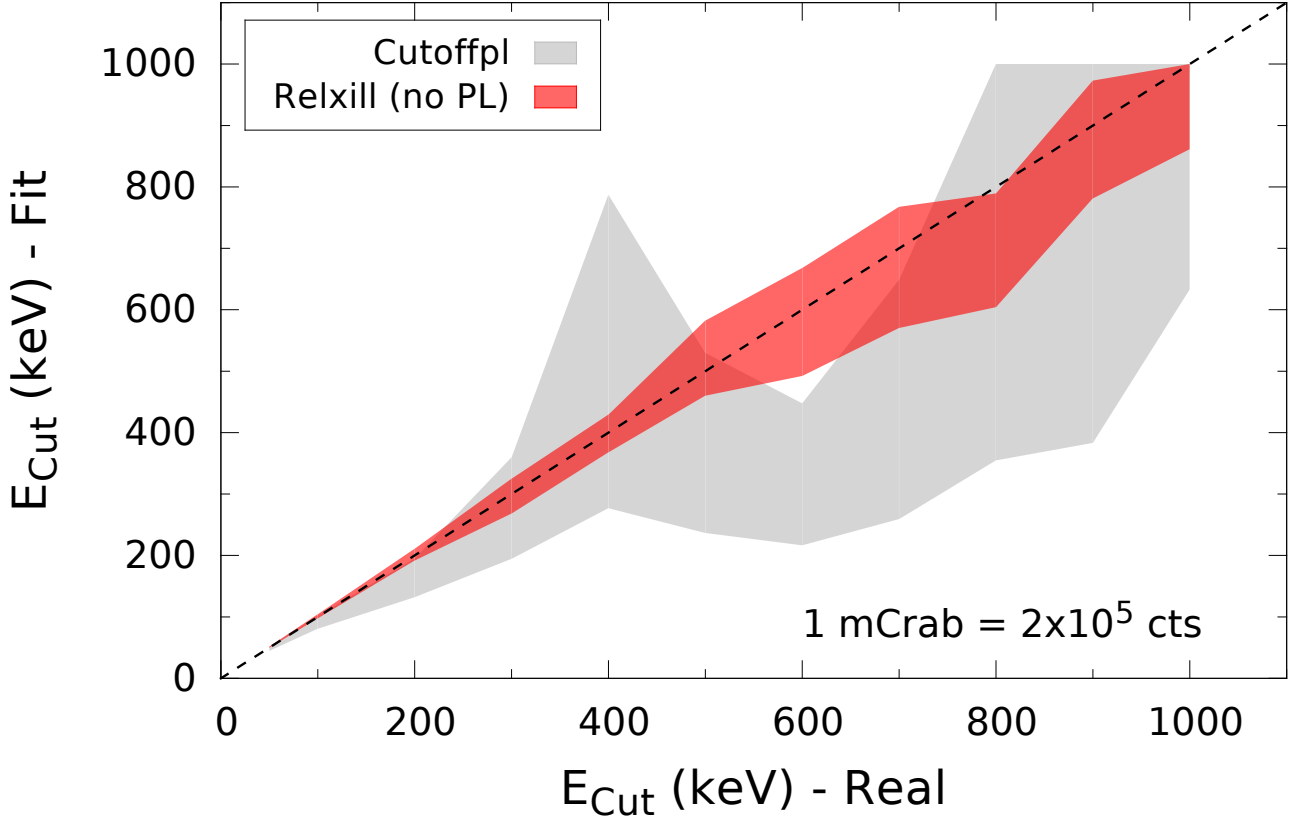


**Figure 5.** Results simulated for a 1 mCrab source demonstrating that a pure reflection model (i.e., no power-law continuum) shown in red is far superior to an e-folded power-law component (i.e., no reflection) in constraining  $E_{\text{cut}}$ .

AGN. (2) However, our simulations indicate that for a simultaneous fit to *Suzaku* and *NuSTAR* data (0.5–79 keV), one can constrain  $E_{\text{cut}}$  for a 1 mCrab source at energies far above the limit of the detector bandpass.

Our results lead to two basic conclusions:

1. In constraining the cutoff energy, misleading results are obtained if the power-law component is cut off externally. It is therefore essential to employ a detailed and accurate model of the reflection spectrum that includes  $E_{\text{cut}}$  as an internal fit parameter.
2. Because the cutoff energy most strongly affects the low-energy part of the reflection spectrum, to obtain useful constraints on  $E_{\text{cut}}$  for AGN it is crucial to combine *NuSTAR* data with low-energy (e.g., *Suzaku* or *XMM-Newton*) data.

This limited study provides only a very cursory exploration of how proper modeling of a reflection spectrum yields useful physical constraints on the high-energy cut-off out to extreme energies. A thorough exploration of the subject is well beyond the scope of this Letter. For example, we illustrate the effects on the reflected spectrum of varying  $E_{\text{cut}}$  for the cases of  $\log \xi = 1$  and 3 (Figure 1) while only presenting simulations for the former case. However, one expects that the effects will be quite different for other choices of the ionization parameter. Moreover, the values of other parameters, such as

the reflection fraction, can affect the statistical significance of the value returned for  $E_{\text{cut}}$ .

JG and JEM acknowledge the support of NASA grant NNX11AD08G. JFS has been supported by NASA Hubble Fellowship HST-HF-51315.01.

## REFERENCES

- Arnaud, K. A. 1996, in *Astronomical Society of the Pacific Conference Series*, Vol. 101, *Astronomical Data Analysis Software and Systems V*, ed. G. H. Jacoby & J. Barnes, 17
- Ballantyne, D. R., Bollenbacher, J. M., Brenneman, L. W., et al. 2014, *ApJ*, 794, 62
- Baloković, M., Matt, G., Harrison, F. A., et al. 2015, *ApJ*, 800, 62
- Brenneman, L. W., Madejski, G., Fuerst, F., et al. 2014, *ApJ*, 788, 61
- Dauser, T., García, J., Parker, M. L., Fabian, A. C., & Wilms, J. 2014, *MNRAS*, 444, L100
- Dauser, T., García, J., Wilms, J., et al. 2013, *MNRAS*, 430, 1694
- Dauser, T., Wilms, J., Reynolds, C. S., & Brenneman, L. W. 2010, *MNRAS*, 409, 1534
- García, J., Dauser, T., Reynolds, C. S., et al. 2013, *ApJ*, 768, 146
- García, J., & Kallman, T. R. 2010, *ApJ*, 718, 695
- García, J., Dauser, T., Lohfink, A., et al. 2014, *ApJ*, 782, 76
- Gierlinski, M., Zdziarski, A. A., Done, C., et al. 1997, *MNRAS*, 288, 958
- Haardt, F. 1993, *ApJ*, 413, 680
- Harrison, F. A., Craig, W. W., Christensen, F. E., et al. 2013, *ApJ*, 770, 103

- Houck, J. C., & Denicola, L. A. 2000, in *Astronomical Society of the Pacific Conference Series*, Vol. 216, *Astronomical Data Analysis Software and Systems IX*, ed. N. Manset, C. Veillet, & D. Crabtree, 591
- Keck, M. L., Brenneman, L. W., Ballantyne, D. R., et al. 2015, *ApJ*, 806, 149
- Marinucci, A., Matt, G., Kara, E., et al. 2014, *MNRAS*, 440, 2347
- Markoff, S., Nowak, M. A., & Wilms, J. 2005, *ApJ*, 635, 1203
- Matt, G., Perola, G. C., Piro, L., & Stella, L. 1992, *A&A*, 257, 63
- Matt, G., Baloković, M., Marinucci, A., et al. 2015, *MNRAS*, 447, 3029
- Parker, M. L., Wilkins, D. R., Fabian, A. C., et al. 2014, *MNRAS*, 443, 1723
- Petrucchi, P. O., Haardt, F., Maraschi, L., et al. 2001, *ApJ*, 556, 716
- Risaliti, G., Harrison, F. A., Madsen, K. K., et al. 2013, *Nature*, 494, 449
- Ross, R. R., & Fabian, A. C. 2005, *MNRAS*, 358, 211
- Rybicki, G. B., & Lightman, A. P. 1979, *Radiative processes in astrophysics* (New York, Wiley-Interscience, 1979. 393 p.)
- Shakura, N. I., & Sunyaev, R. A. 1973, *A&A*, 24, 337
- Titarchuk, L. 1994, *ApJ*, 434, 570
- Walton, D. J., Nardini, E., Fabian, A. C., Gallo, L. C., & Reis, R. C. 2013, *MNRAS*, 428, 2901
- Wardziński, G., Zdziarski, A. A., Gierliński, M., et al. 2002, *MNRAS*, 337, 829
- Wilms, J., Allen, A., & McCray, R. 2000, *ApJ*, 542, 914
- Zdziarski, A. A., Lubiński, P., Gilfanov, M., & Revnivtsev, M. 2003, *MNRAS*, 342, 355
- Zdziarski, A. A., Lubiński, P., & Smith, D. A. 1999, *MNRAS*, 303, L11
- Zdziarski, A. A., Poutanen, J., & Johnson, W. N. 2000, *ApJ*, 542, 703